AFRL-RX-WP-TP-2011-4291

THE STRENGTH OF CHEMICAL BONDS IN SOLIDS AND LIQUIDS (PREPRINT)

Daniel B. Miracle

Metals Branch
Metals, Ceramics, and NDE Division

Garth B. Wilks

General Dynamics Corporation

Amanda Dahlman and James Dahlman

Southwestern Ohio Council for Higher Education (SOCHE)

JULY 2011

Approved for public release; distribution unlimited.

See additional restrictions described on inside pages

STINFO COPY

AIR FORCE RESEARCH LABORATORY
MATERIALS AND MANUFACTURING DIRECTORATE
WRIGHT-PATTERSON AIR FORCE BASE, OH 45433-7750
AIR FORCE MATERIEL COMMAND
UNITED STATES AIR FORCE

REPORT DOCUMENTATION PAGE

Form Approved
OMB No. 0704-0188

1. REPORT DATE ***(DD-MM-YY)***
July 2011

2. REPORT TYPE
Journal Article Preprint

3. DATES COVERED *(From - To)*
01 July 2011 – 01 July 2011

4. TITLE AND SUBTITLE
THE STRENGTH OF CHEMICAL BONDS IN SOLIDS AND LIQUIDS (PREPRINT)

5a. CONTRACT NUMBER
In-house

5b. GRANT NUMBER

5c. PROGRAM ELEMENT NUMBER
62102F

6. AUTHOR(S)
D.B. Miracle (AFRL/RXLM)
Garth B. Wilks (General Dynamics Corporation)
Amanda Dahlman and James Dahlman (SOCHE)

5d. PROJECT NUMBER
4347

5e. TASK NUMBER
20

5f. WORK UNIT NUMBER
LM10512P

7. PERFORMING ORGANIZATION NAME(S) AND ADDRESS(ES)

Metals Branch (AFRL/RXLM)
Metals, Ceramics, and NDE Division
Air Force Research Laboratory, Materials and Manufacturing Directorate
Wright-Patterson Air Force Base, OH 45433-7750
Air Force Materiel Command, United States Air Force

General Dynamics Corporation
Dayton, OH 45431

Southwestern Ohio Council for Higher Education (SOCHE)
Dayton, OH 45420

8. PERFORMING ORGANIZATION REPORT NUMBER
AFRL-RX-WP-TP-2011-4291

9. SPONSORING/MONITORING AGENCY NAME(S) AND ADDRESS(ES)
Air Force Research Laboratory
Materials and Manufacturing Directorate
Wright-Patterson Air Force Base, OH 45433-7750
Air Force Materiel Command
United States Air Force

10. SPONSORING/MONITORING AGENCY ACRONYM(S)
AFRL/RXLM

11. SPONSORING/MONITORING AGENCY REPORT NUMBER(S)
AFRL-RX-WP-TP-2011-4291

12. DISTRIBUTION/AVAILABILITY STATEMENT
Approved for public release; distribution unlimited.

13. SUPPLEMENTARY NOTES
PAO Case Number: 88ABW 2010-2016; Clearance Date: 13 Apr 2010. Document contains color.
Journal article submitted to *Acta Materialia.*

14. ABSTRACT
The strengths of chemical bonds between atoms are accurately measured and widely available for molecular gases, but it is remarkable that a method to quantify bond strengths in liquids and solids is not available and that the strengths of these bonds are generally unknown. We propose a new term, the condensed bond enthalpy (CBE), to specify the energy contained in bonds between atoms in condensed states. We develop an approach to quantify these bond strengths using bulk thermodynamic and crystallographic data, and apply it to generate a nearly complete set of elemental CBEs and a selection of CBEs between unlike metal atom pairs. We demonstrate the validity and utility of these values by applying them to several physical problems. The values reported here show a good predictive capability, and CBEs from this approach may give new insights into solution thermodynamics and emerging problems in the physical sciences.

15. SUBJECT TERMS
molecular gases, condensed bond enthalpy (CBE), bulk thermodynamic, crystallographic data, thermodynamics

16. SECURITY CLASSIFICATION OF: a. REPORT	b. ABSTRACT	c. THIS PAGE	17. LIMITATION OF ABSTRACT:	18. NUMBER OF PAGES
Unclassified	Unclassified	Unclassified	SAR	42

19a. NAME OF RESPONSIBLE PERSON (Monitor)
Jonathan E. Spowart

19b. TELEPHONE NUMBER *(Include Area Code)*
N/A

The strength of chemical bonds in solids and liquids

Daniel B. Miracle[1*], Garth Wilks[1,2], Amanda Dahlman[1,3] & James Dahlman[1,3†]

[1]*Air Force Research Laboratory, Materials and Manufacturing Directorate, Wright-Patterson AFB, OH 45433 USA*

[2]*General Dynamics Corporation, Dayton, OH 45431 USA*

[3]*Southwestern Ohio Council for Higher Education (SOCHE), Dayton, OH 45420 USA*

[*]*email: daniel.miracle@wpafb.af.mil*

[†]*Present address: Harvard-MIT Division of Health Sciences, Massachusetts Institute of Technology, 77 Massachusetts Avenue, Cambridge, MA 02139 USA*

The strengths of chemical bonds between atoms are accurately measured and widely available for molecular gases, but it is remarkable that a method to quantify bond strengths in liquids and solids is not available and that the strengths of these bonds are generally unknown. We propose a new term, the condensed bond enthalpy (CBE), to specify the energy contained in bonds between atoms in condensed states. We develop an approach to quantify these bond strengths using bulk thermodynamic and crystallographic data, and apply it to generate a nearly complete set of elemental CBEs and a selection of CBEs between unlike metal atom pairs. We demonstrate the validity and utility of these values by applying them to several physical problems. The values reported here show a good predictive capability, and CBEs from this approach may give new insights into solution thermodynamics and emerging problems in the physical sciences.

Current Bond Strength Representations

The strengths of chemical bonds between atoms exerts decisive control in a wide range of physical phenomena, including the stability and structure of matter; the kinetics of chemical reactions and the energy required or produced in the formation of alloys and compounds. Bond strengths are commonly quantified by terms such as bond dissociation energy (BDE) and bond enthalpy. Approaches to accurately measure these values, typically to four significant figures, are well-established [1], and extensive tabulations are available for a wide range of elements and compounds [2,3,4,5]. While these values have a strong and demonstrated utility, they are defined and measured only for species in the gaseous state, and are likely to differ significantly from single bond strengths between atoms in liquids and solids. A companion approach to accurately quantify interatomic bond strengths in the condensed state does not currently exist, leading to the condition that surprisingly little quantitative data is available for the strengths of chemical bonds in liquids and solids.

The minimum in the atomic potential energy vs separation curve gives a simple representation of bond strength. Atomic potentials are often used in semi-empirical computational approaches. They are produced by fitting to measured values that include elastic properties, defect energies and structural data, and so give an indirect approach that can require extensive auxiliary information. Pair potentials with as few as two fitting parameters are used for simplicity, while more realistic potentials use as many as 14 fitting parameters [6]. Consequently, realistic, high quality atomic potentials are difficult to produce and validate, even in binary systems. Quantitative comparison of energies across systems requires a uniform approach for producing atomic potentials, but fitting techniques are often unique so that caution must be used in such comparisons. *Ab initio* calculations can give accurate total energies in condensed structures, but it is difficult to assign individual bond strengths to specific atomic pairs. Both first principles and semi-empirical calculations can be rather involved, and it has

been difficult to perform calculations on enough systems to establish trends and patterns, which are only now just beginning to emerge [7]. Extensive efforts to predict phase equilibria in condensed systems give phenomenological representations of thermodynamic functions, including composition-dependent enthalpies and atomic interaction parameters [8]. However, these approaches have not been used to define and quantify chemical bond strengths. The regular solution and quasi-chemical models have their foundations in bond energies between like and unlike atom pairs in condensed substances, ε_{ij}, and form a framework for the application and interpretation of these values [9,10]. To our knowledge, ε_{ij} values have not been quantified using a thermodynamics approach.

Elemental Condensed Bond Enthalpies

We develop here an approach for estimating bond enthalpies in condensed elements. The conversion of one mole of pure, condensed element *A* to a non-interacting, monatomic gas requires a change in enthalpy that is given as the difference between the enthalpies of the products and reactants

$$\Delta_f H(A,gas) = H(A,gas) - H(A,cond) \tag{1}$$

This change can be measured as the heat of formation of a monatomic gas, which is numerically equal to the heat of sublimation for solid elements that convert to a monatomic gas. Experimental values are typically given at 298 K and atmospheric pressure (100 kPa) [4,5,11,12]. Only changes in thermodynamic values can be measured, so an enthalpy of $H(A,gas) = 0$ is assigned for convenience to the non-interacting, monatomic gas as the reference state against which changes are quantified. This assignment is consistent with the reference state typically used for atomic potential functions, and has the advantage of enabling distinction between different elements at 298 K. This differs from the ‘elemental’ standard state often used in classical

thermodynamics, $H(A,cond) = 0$, which eliminates the ability to distinguish between different elements in the condensed state since all are assigned a zero enthalpy. We use the foundational relation of the regular solution and quasi-chemical models [9,10]

$$H = \sum_{i,j} \varepsilon_{ij} P_{ij} \tag{2}$$

where ε_{ij} is the enthalpy of an *i-j* atomic bond and P_{ij} is the number of first-neighbour *i-j* bonds. Applying the previous equations to one mole of pure element A gives

$$H(A,cond) = -\Delta_f H(A,gas) = \varepsilon_{AA}(P_{AA}) = \varepsilon_{AA}(N_{Av}Z_{AA})/2 \tag{3}$$

where N_{Av} is Avogadro's constant. The number of bonds per mole of atoms, P_{AA}, is proportional to half the coordination number, Z_{AA}, to avoid counting a bond twice. Rearranging terms gives

$$\varepsilon_{AA} = -2\Delta_f H(A,gas)/(N_{Av}Z_{AA}) \tag{4}$$

We use $\Delta_f H(gas)$ values assessed from data in [4,5,11,12] (see Supplementary Information, Table S1). $\Delta_f H(gas)$ is a positive energy, so that ε_{AA} is negative. For convenience, we report ε_{AA} in units of eV. We determine ε_{AA} for all elements, excluding noble gases, Pm, At, Fr and elements with atomic number greater than 94 where required input data are unavailable (Table 1). Bond enthalpies typically range from −0.1 eV to −1.5 eV, with values as large as −4.95 eV for elements where covalent bonding dominates. These values are broadly consistent with expected bond energies [13] and show a clear dependence on melting temperature, T_m (Figure 1). Semi-metal and non-metal elements are dominated by covalent bonding and have coordination numbers much less than 12, giving strongly negative ε_{AA} values (Figure 1a). However, all elements follow the same trend when the same coordination number– a space-filling coordination of 12– is used to calculate ε_{AA} (Figure 1b). Consistent with Equation 4, the correlations in Figure 1 suggest that an atom has a specific capacity for bonding, given

by $\Delta_f H(gas)$, and that the strength of the bond depends on the number of bonds formed. This observation gives an approach to quantify the influence of atomic structure, by adjusting bond strengths by the number of bonds per atom in the structure.

Quantitative validation of these bond enthalpies is given by comparing measured vacancy formation energies, enthalpies of fusion and surface energies with values predicted from ε_{AA}. The energy to form a monovacancy in a pure element, ΔH_{1v}, is modelled as the product of ε_{AA} and the net change in bonds needed to form this defect. Removing an atom from a solid interior breaks six bonds in face-centered cubic (fcc) and hexagonal close-packed (hcp) structures, and breaks seven bonds in body-centred cubic (bcc) structures. This atom is placed on a free surface to maintain mass balance, and the number of new bonds formed depends on the crystallographic plane and the site occupied. Surface sites include atomically smooth surfaces, atomic ledges, kinks and surface vacancies. Filling a surface vacancy forms the largest number of new bonds, so this site has the lowest energy and is strongly preferred. We count the number of new bonds for filled surface vacancies on (100), (110) and (111) planes in fcc structures, for (0001), $(10\bar{1}0)$, $(11\bar{2}0)$ and $(11\bar{2}1)$ planes in hcp structures, and on (100), (110) and (112) planes in bcc structures. The average number of new bonds formed is 4 for fcc and hcp structures and 4.5 for bcc structures. We apply a small correction to account for the redistribution of electrons associated with broken bonds at defect sites (see Methods). The results in Figure 2 show that the predicted energies are typically within experimental error.

As a second application of ε_{AA}, we consider the enthalpy of fusion, ΔH_m, which accompanies the transformation from the crystal to liquid state at T_m. This enthalpy change can be estimated as

$$\Delta H_m = -\varepsilon_{AA}^{T_m}\left(\frac{\Delta Z}{2}\right) N_{Av} \tag{5}$$

where $\varepsilon_{AA}^{T_m}$ is the enthalpy of an A–A bond at T_m and $\Delta Z/2$ is the change in the number of bonds per atom associated with melting. To obtain $\varepsilon_{AA}^{T_m}$, we adjust $\Delta_f H(A,gas)$ by the enthalpy required to heat the element to T_m (see Methods). This reduces ε_{AA} by about 10%. We perform estimates for fcc and hcp metals that do not undergo allotropic transformations, using ΔZ=0.7 as measured for liquid Cu [14]. A small adjustment to ε_{AA} due to charge redistribution at broken bonds (see Methods) is applied. Predicted values of ΔH_m plotted against experimental values in Figure 3 show good agreement, again typically within experimental uncertainty.

The final application of ε_{AA} values given here is for solid surface energies, γ. Surface energies are represented by the number of bonds broken per unit area (see Supplementary Information) and the enthalpy of those broken bonds (see Methods). Surface energies are predicted for (100), (110) and (111) planes in fcc crystals and for (100), (110) and (112) planes in bcc elements. For each element, the mean of the predicted values are compared with γ for cubic metals measured by the zero creep method at elevated temperatures [15]. Predictions for eight elements show very good agreement with values measured at 1723 K or below and at 0.77 T_m or above (Figure 4). Estimates significantly exceed measured values for Nb, Mo and W, where much higher measurement temperatures, from 2273 to 2623 K, are used. Enhanced adsorption of impurity atoms at these higher temperatures may contribute to the poor agreement for these measurements.

Condensed Bond Enthalpies Between Unlike Atom Pairs

Consider the reaction of x moles of pure, condensed element A with y moles of element B to form one mole of the compound A_xB_y at standard temperature and pressure. The enthalpy of formation can be measured experimentally, and is

$$\Delta_f H(A_xB_y) = H(A_xB_y) - xH(A,cond) - yH(B,cond) \tag{6}$$

We expand $H(A_xB_y)$ using Equation 2

$$H(A_x B_y) = \varepsilon_{AA} P_{AA}^{A_x B_y} + \varepsilon_{AB} P_{AB}^{A_x B_y} + \varepsilon_{BB} P_{BB}^{A_x B_y} \tag{7}$$

where $P_{ij}^{A_x B_y}$ is the number of i–j bonds per mole of A_xB_y. We replace $H(i,cond)$ with $-\Delta_f H(i,gas)$ and rearrange terms to give the basic relation

$$\varepsilon_{AB} = \left(\frac{1}{P_{AB}^{A_x B_y}}\right) \left\{\left[\Delta_f H(A_x B_y) - x\Delta_f H(A,gas) - y\Delta_f H(B,gas)\right] - \varepsilon_{AA} P_{AA}^{A_x B_y} - \varepsilon_{BB} P_{BB}^{A_x B_y}\right\} \tag{8}$$

This is modified (see Methods) to give our final equation

$$\varepsilon_{AB} = \left(\frac{1}{p_{AB}^{A_x B_y}}\right)\left\{\left(\frac{U}{N_{Av}(x+y)}\right)\left[\Delta_f H(A_x B_y) - x\Delta_f H(A,gas) - y\Delta_f H(B,gas)\right] - \varepsilon_{AA}^{A_x B_y}\left(p_{AA}^{A_x B_y}\right) - \varepsilon_{BB}^{A_x B_y}\left(p_{BB}^{A_x B_y}\right)\right\} \tag{9}$$

The terms ε_{ii} are replaced with $\varepsilon_{ii}^{A_x B_y}$ to indicate a small dependence of like-atom bond enthalpy on structure. $P_{ij}^{A_x B_y}$ is replaced with $p_{ij}^{A_x B_y}$, the number of i–j bonds per unit cell of A_xB_y. The approach for counting bonds per unit cell is given in Methods. U is the number of atoms per unit cell in the A_xB_y structure. The experimentally measured quantities, $\Delta_f H(A_xB_y)$ [16,17,18,19] and $\Delta_f H(i,gas)$ [4,5,11,12], are converted to units of eV for convenience.

We determine ε_{AB} for eleven binary systems where available data give a minimum of four values for each system to establish compositional trends. We include data for four additional binary systems with fewer than four values, which are used to predict heats of formation for ternary intermetallic compounds from ε_{AB}. We focus on binary metallic systems in response to Pauling's complaint that "the great field of chemistry comprising the compounds of metals with one another has been largely neglected by chemists in the past" [20]. For consistency, the element B is chosen so that ε_{BB} is more

negative than ε_{AA}. Results are shown in Figure 5, and values are tabulated in Supplementary Information, Table S4.

ε_{AB} values satisfy general expectations. Since compounds are formed in each of the binary systems studied here, a negative deviation from ideal solid solutions is expected. Consistent with this, ε_{AB} never exceeds $(\varepsilon_{AA} + \varepsilon_{BB})/2$, the criterion for ideal solid solutions. ε_{AB} also does not exceed the weighted average of $\varepsilon_{AA}^{A_xB_y}$ and $\varepsilon_{BB}^{A_xB_y}$ (Al-Nb is an exception) and it intersects this weighted average at the atom fraction of element B, f_B, of the most solute-rich compound in that binary system. ε_{AB} usually falls between $\varepsilon_{AA}^{A_xB_y}$ and $\varepsilon_{BB}^{A_xB_y}$, but is sometimes more negative than both of these values. Finally, ε_{AB} values calculated from Equation 9 using the 'elemental' standard state (commonly used in classical thermodynamics, where $\varepsilon_{ii} = 0$) are essentially independent of f_B. We validate the unlike atom bond energies by predicting enthalpies of formation for ternary compounds, $\Delta_f H(A_xB_yC_z)$, from $\varepsilon_{ii}^{A_xB_y}$ and ε_{ij} and from the numbers of i–j bonds per mole of $A_xB_yC_z$, $P_{ij}^{A_xB_yC_z}$ (see Methods). Agreement is good, and is generally within experimental error (Figure 6). Additional data supporting this comparison is given in Supplementary Information, Table S5.

To our knowledge, there are very few published values against which these condensed bond enthalpies can be compared. Atomic potentials for the Ni-Zr system [21] give ε_{NiNi} and ε_{ZrZr} that are between one half and two thirds of the values determined here, and give ε_{NiZr} values that range from 0.62 to 1.03 of the present values. Other potentials seem to give values that are much lower [22]. The crystal orbital Hamiltonian population (COHP), although not a bond strength in the manner discussed here, is nevertheless an indication of the covalent contribution to interatomic bonding [23]. COHP values for Fe-Fe bonding range from one half to twice the value reported here for ε_{FeFe}, and values for metal-metalloid bonding range from about -2 eV to -3.5 eV [23,24]. Bond dissociation enthalpies for diatomic gaseous elements [3] generally range from about 3

times smaller to 4 times larger than the ε_{ii} values for condensed elements, consistent with the expectation that these values may not be comparable [5].

ε_{AB} is relatively insensitive to composition when $\varepsilon_{AA}{\approx}\varepsilon_{BB}$, but shows a mild dependence on f_B when ε_{BB} is significantly more negative than ε_{AA}. In these systems, ε_{AB} is typically more negative for A–rich compounds and becomes slightly less negative with increasing f_B. It is possible that B–B bonds are increasingly preferred as ε_{BB} becomes more negative than ε_{AA}, but an analysis of the fractions of A–A, A–B and B–B bonds in the studied intermetallic structures does not conclusively support this idea. The fractions of bonds between like and unlike atom pairs are, however, consistently influenced by atom size. Relative to the fractional number of bonds expected for an ideal, random binary solution of equal-sized atoms [9], there are fewer bonds between the smaller atoms across the entire range of f_B, there are more bonds between unlike atoms for compounds rich in the smaller atom, and there are more bonds between the larger atoms for compounds rich in the larger atom (see Supplementary Information, Figure S1). These trends are consistent with simple topological arguments and with a general size dependence acknowledged in conventional thermodynamics. The present work gives explicit relations between numbers of bonds and ε_{ij}, but, to our knowledge, the relationships between atomic structure (and hence the frequency of A–A, A–B and B–B bonds), topology (atom size) and the relative values of ε_{AA}, ε_{AB} and ε_{BB} are not clearly understood and bear further study.

The present approach offers the simplicity of pair interactions, but higher-order energy terms are embedded in the bond enthalpies reported here, since changes in *total* enthalpies are used to calculate ε_{ij}. The magnitude of higher-order bond interactions can be estimated through analysis of stacking fault energies, which arise from a change in second-neighbour bonding. Assigning measured stacking fault energies [25] to the bonds across a stacking fault defect and normalizing by ε_{ii} shows that second-neighbour

interactions typically range from 0.5-5% of ε_{ii} for fcc metallic elements and from 6-16% for hcp metals (see Supplementary Information, Table S6). Measurement errors for $\Delta_f H(A,gas)$ and $\Delta_f H(A_xB_y)$ give an average uncertainty in ε_{ij} of about ±3%, and this is suggested as a basic limit in precision of ε_{ij} values given here. For unusual cases where the first coordination shell of the relevant crystal structure is ambiguous (see Methods), ε_{ij} errors can be as large as ±10%.

Standard treatments of solution models emphasize the difference between ε_{AB} and the average of ε_{AA} and ε_{BB}, but the importance of relative differences between ε_{AA} and ε_{BB} are rarely discussed. The 'elemental' standard state does not allow distinction between ε_{AA} and ε_{BB}, while this difference can be quantified with the gas standard state. The structure and stability of condensed phases may depend on the relative magnitudes of ε_{AA}, ε_{AB} and ε_{BB}, so that the gas standard state used here for ε_{ij} is likely to be useful for understanding complex, multi-component substances including 'superalloys' that can contain as many as a dozen elements, high entropy alloys [26] and metallic glasses [27,28].

Although the current approach is applied here only to metallic systems, it may be more generally useful for other condensed, inorganic substances including compounds of metal/semi-metal and metal/non-metal atoms. It may also be useful in condensed materials where ionic bonding dominates, as ionic bonding is non-directional and often produces efficiently packed atomic structures with high coordination numbers. It is not certain at present if covalent materials may be treated with appropriate adaptations of the methods developed here. Adjustment of bond energies based on the local atomic coordination in the substance of interest gives good results in the present work for extending bond enthalpies from elements to binary compounds and from binary to ternary compounds, and is a suggested approach.

Condensed bond enthalpies are vital companions to bond dissociation enthalpies, and may provide a similar impact to the understanding of liquid and solid substances and their reactions. Condensed bond enthalpies can give essential insights into the structure and stability of complex systems, such as ternary and higher order inorganic compounds, amorphous metals, and high entropy alloys, where structural complexity challenges current modeling approaches, and where insights are likely to come from trends established by the study of many systems rather than detailed investigations in a small number of selected systems. Condensed bond enthalpies are also expected to give new insights into the kinetics of chemical reactions such as catalysis and the fragility of liquids [29], where the relative magnitudes of bond energies at a local atomic scale are important. Condensed bond enthalpies provide new data to support the established field of solution thermodynamics and may give new insights by quantifying differences between ε_{AA} and ε_{BB}. Finally, observations in the present work link chemistry and structural topology, suggesting an intriguing approach to combine topology and energy of atomic structures in liquids and solids.

METHODS

Enthalpy of broken bonds. Cohesive energy is intimately connected to the spatial distribution of electrons [30]. The redistribution of electrons at defects [31] is thus expected to alter the enthalpy of the broken bonds associated with those defects. Consider the redistribution of electrons associated with bond breaking: electrons in the initial bond become partitioned between the broken, or 'dangling', bond and the bonds that remain intact around the defect site. We propose a simple estimate of this partitioning, where the fraction of enthalpy remaining in the broken bond is equal to the fractional coordination number of atoms in the first coordination shell of the defect. This correction is simplest for free surfaces. Surface atoms on $(111)_{fcc}$ planes have a coordination of 9 and an initial coordination number of 12, so that the fractional

enthalpy remaining in the broken bonds is 3/4. The fraction is 2/3 for $(100)_{fcc}$ planes and 3/4 for $(110)_{fcc}$ planes, giving an average fractional enthalpy of 13/18 (about 0.722) for broken bonds associated with low-index fcc planes. Fractional coordinations for surface atoms are 5/7 (about 0.714) for each of the $(100)_{bcc}$, $(110)_{bcc}$ and $(112)_{bcc}$ planes.

The correction for the enthalpy of broken bonds at a vacancy requires terms for atoms surrounding both the site where the atom is removed and where it is placed on the surface. The twelve atoms surrounding a vacant site in an fcc structure have a final coordination of 11 and an initial coordination of 12. Placing the displaced atom in a surface vacancy on a $(111)_{fcc}$ plane changes its coordination number from 12 to 9, changes the coordination number for the three atoms at the bottom of the surface vacancy from 11 to 12, and changes the coordination number from 8 to 9 for the six remaining atoms that form the surface vacancy. The average change in coordination number for the atoms associated with this defect is thus

$$\frac{12(11/12)+1(9/12)+3(12/11)+6(9/8)}{22} = 0.990. \quad \text{(M1)}$$

Similar analysis gives fractions of 0.981 for $(100)_{fcc}$ planes and 0.970 for $(110)_{fcc}$ planes, for an average of 0.980 for low-index surfaces in the fcc structure. Average corrections are 0.981 for $(100)_{bcc}$, $(110)_{bcc}$ and $(112)_{bcc}$ planes and 0.981 for $(0001)_{hcp}$, $(10\bar{1}0)_{hcp}$, $(10\bar{1}1)_{hcp}$ and $(11\bar{2}1)_{hcp}$. planes.

A similar correction is made to account for the bonds broken upon melting. The change in coordination occurs equally, in a stochastic sense, for all atoms. Only fcc and hcp structures are considered here, so that the initial coordination number is 12, the final coordination number is Z–ΔZ = 11.3 and the fractional enthalpy retained in the broken bonds is 0.942.

Temperature adjustment of ε_{AA}. The enthalpy content of a solid at 298 K in the present work, -$\Delta_f H(A,gas)$, becomes less negative as the solid is heated above this temperature. This enthalpy reduction is (H_{T_m}-H_{298}) at the melting temperature, so that

$$\varepsilon_{AA}^{T_m} = \varepsilon_{AA}\left[1 - \frac{(H_{T_m} - H_{298})}{\Delta_f H(A,gas)}\right] \quad \text{(M2)}$$

When available, tabulated values of (H_{T_m}-H_{298})[18] are used in the present analyses. When they are not available, $\varepsilon_{AA}^{T_m}$ is estimated as

$$\varepsilon_{AA}^{T_m} = \varepsilon_{AA}\left[1 - \frac{C_p(T_m - 298)}{\Delta_f H(A,gas)}\right] \quad \text{(M3)}$$

where C_p is the elemental heat capacity.

Surface energies. The surface energy, γ, is given as [15]

$$\gamma = F_s = E_s - TS_s \quad \text{(M4)}$$

where F, E and S are the Helmholtz free energy, internal energy and entropy and the subscript, s, indicates properties at a free surface. The internal energy is estimated as

$$E_s = -\text{Б}(\varepsilon_{AA}^{T_{meas}}) = -\text{Б}(\varepsilon_{AA})\left[1 - \frac{(H_{T_{meas}} - H_{298})}{\Delta_f H(A,gas)}\right] \quad \text{(M5)}$$

where $Б$ is the number of bonds per unit area. $\varepsilon_{AA}^{T_{meas}}$ is the bond enthalpy at the temperature which the surface energy is measured, T_{meas}, and is determined as described above for $\varepsilon_{AA}^{T_m}$. The surface entropy is evaluated by taking the temperature derivative of F_s and rearranging terms

$$S_s = \left[\frac{(\text{Б})(\varepsilon_{AA})}{\Delta_f H(A,gas)}\right]\left[\frac{d(H_T - H_{298})}{dT}\right] - \frac{dF_s}{dT} \quad \text{(M6)}$$

The temperature dependence of $(H_T - H_{298})$ is determined using tabulated data [18] from temperatures just above (T2) and just below (T1) the measurement temperature, so that

$$S_s = \left[\frac{(Б)(\varepsilon_{AA})}{\Delta_f H(A,gas)}\right]\left[\frac{(H_{T2}-H_{298})-(H_{T1}-H_{298})}{T2-T1}\right] - \frac{dF_s}{dT} \quad \text{(M7)}$$

Measured values of $d\,F_s/dT$ are given in [15]. The surface energy is calculated by inserting Equations M5 and M7 into Equation M4. The value of ε_{AA} used here includes correction for the change in coordination number associated with bonds broken upon melting, as described earlier in Methods. Tabulated values of $Б$ (Table S2) and of data used in the calculation of γ (Table S3) are given in Supplementary Information.

Calculation of ε_{AB}. Bond counting and adjustment of ε_{ii} to account for the different structures in the element and the compound are used to transform Equation 8 for ε_{AB} into Equation 9. Crystallographic data enable bond counting. The Pearson symbol for the equilibrium structure [32,33] points to detailed information of the unit cell [34]. The numbers of A–A, A–B and B–B bonds between the central atom and each of the atoms in the first coordination shell are counted for each of the constituent polyhedra in the unit cell. These values are multiplied by appropriate site occupancies and site multiplicities, and the sums are halved to avoid double-counting of bonds. The resulting numbers of bonds per unit cell of A_xB_y, $p_{ij}^{A_xB_y}$ are converted to the number bonds per mole of A_xB_y, $P_{ij}^{A_xB_y}$ via

$$P_{ij}^{A_xB_y} = \left(\frac{N_{Av}(x+y)}{U}\right) p_{ij}^{A_xB_y} \quad \text{(M8)}$$

Here x and y are the numbers of A and B atoms, respectively, in the A_xB_y formula unit and U is the number of atoms per unit cell. While polyhedral coordination numbers in [34] are usually reliable, in rare cases apparent discrepancies exist. We perform a critical assessment of the coordination number for each polyhedron to include atoms up to a distance of 1.25 times the minimum atomic separation for each of the A–A, A–B and B–B atom pairs. Where a discrepancy between reported and assessed coordination numbers is found, we use the average of the two values with an associated error in $p_{ij}^{A_xB_y}$. This results in a larger error for ε_{AB}.

We propose that bond enthalpy depends on structure via the number of bonds formed per atom, as suggested by Figure 1b. Thus, the more bonds formed per atom, the lower is the enthalpy per bond. We apply a simple estimate of this effect

$$\varepsilon_{ii}^{A_xB_y} = \left(\frac{\overline{p}^{elem}}{\overline{p}^{A_xB_y}}\right)\varepsilon_{ii} \tag{M9}$$

where $\overline{p}^{elem} = Z_{AA}/2$ is the average number of bonds per atom in the pure element, and $\overline{p}^{A_xB_y} = \left(\frac{1}{U}\right)\left(p_{AA}^{A_xB_y} + p_{AB}^{A_xB_y} + p_{BB}^{A_xB_y}\right)$ is the average number of bonds per atom in the A_xB_y structure. $\overline{p}^{elem}$ is usually either 6 (for fcc and hcp) or 7 (for bcc), while $\overline{p}^{A_xB_y}$ is typically between 6 and 7. A similar correction is applied for ternary compounds,

$$\varepsilon_{ii}^{A_xB_yC_z} = \left(\frac{\overline{p}^{elem}}{\overline{p}^{A_xB_yC_z}}\right)\varepsilon_{ii} \tag{M10a}$$

$$\varepsilon_{AB}^{A_xB_yC_z} = \left(\frac{\overline{p}^{A_xB_y}}{\overline{p}^{A_xB_yC_z}}\right)\varepsilon_{AB}, \quad \varepsilon_{AC}^{A_xB_yC_z} = \left(\frac{\overline{p}^{A_xC_z}}{\overline{p}^{A_xB_yC_z}}\right)\varepsilon_{AC}, \quad \varepsilon_{BC}^{A_xB_yC_z} = \left(\frac{\overline{p}^{B_yC_z}}{\overline{p}^{A_xB_yC_z}}\right)\varepsilon_{BC} \tag{M10b}$$

where $\overline{p}^{A_xB_y}$ is determined for the binary compound at the same ratio of x:y as in the ternary, or as the weighted average of the binary compounds that bracket this composition. ε_{AB} is determined by inserting $f_B = x/(x+y)$ into a linear regression of ε_{AB} vs. f_B from the appropriate binary systems.

Enthalpies of ternary compounds. The formation enthalpy of a ternary compound, $A_xB_yC_z$, is

$$\Delta_f H(A_xB_yC_z) = H(A_xB_yC_z) - xH(A, cond) - yH(B, cond) - zH(C, cond) \tag{M11}$$

Expanding $H(A_xB_yC_z)$ and substituting $-\Delta_f H(i, gas)$ for $H(i, cond)$ gives

$$\Delta_f H(A_xB_yC_z) = P_{AA}^{A_xB_yC_z}\varepsilon_{AA}^{A_xB_yC_z} + P_{AB}^{A_xB_yC_z}\varepsilon_{AB}^{A_xB_yC_z} + P_{AC}^{A_xB_yC_z}\varepsilon_{AC}^{A_xB_yC_z} + P_{BB}^{A_xB_yC_z}\varepsilon_{BB}^{A_xB_yC_z} + P_{BC}^{A_xB_yC_z}\varepsilon_{BC}^{A_xB_yC_z} + P_{CC}^{A_xB_yC_z}\varepsilon_{CC}^{A_xB_yC_z} + x\Delta_f H(A, gas) + y\Delta_f H(B, gas) + z\Delta_f H(C, gas) \tag{M12}$$

Citations.

1 Cottrell, T. L. *The Strengths of Chemical Bonds*. (Butterworths Scientific Publications, 1958).

2 Darwent, B. d. Bond Dissociation energies in Simple Molecules. (National Bureau of Standards, US Department of Commerce, Washington DC, 1970).

3 Dean, J. A. *Lange's Handbook of Chemistry*. 15th edn, (McGraw-Hill Inc., New York, NY, 1999).

4 *CRC Handbook of Chemistry and Physics*. 88th edn, (ed D.R. Lide) (CRC Press, Boca Raton, FL USA, 2008).

5 Winter, M. *WebElements: the periodic table on the WWW*, <http://www.webelements.com/> (2009).

6 Kim, Y.-M. & Lee, B.-J. A modified embedded-atom method interatomic potential for the Cu-Zr system. *J. Mater. Res.* **23**, 1095-1104 (2008).

7 Curtarolo, S., Morgan, D. & Ceder, G. Accuracy of *ab initio* methods in predicting the crystal structures of metals: A review of 80 binary alloys. *Computer Coupling of Phase Diagrams and Thermochemistry* **29**, 163-211 (2005).

8 Chang, Y. A. *et al.* Phase diagram calculation: past, present and future. *Prog. Mat. Sci.* **49**, 313-345 (2004).

9 Gaskell, D. R. *Introduction to the Thermodynamics of Materials*. 3rd edn, 134,135 (Taylor & Francis, 1995).

10 Lupis, C. H. P. *Chemical Thermodynamics of Materials*. (Elsevier Science Publishing Co., Inc., 1983).

11 Cox, J. D., Wagman, D. D. & Medvedev, V. A. *CODATA Key Values for Thermodynamics*. Vol. 2009 (Hemisphere Publishing Corp., New York, NY USA, 1989).

12 Teatum, E., K. Gschneidner, J. & Waber, J. Compilation of calculated data useful in predicting metallurgical behavior of the elements in binary alloy systems. Report No. LA-2345, (Los Alamos National Laboratory, University of California, Los Alamos, New Mexico, 1960).

13 Spaepen, F. A survey of energies in materials science. *Phil. Mag.* **85**, 2979-2987 (2005).

14 Lamparter, P. & Steeb, S. in *Structure of Solids* Vol. Volume 1 *Materials Science and Technology, A Comprehensive Treatment* (ed V. Gerold) 217-288 (VCH, 1993).

15 Murr, L. E. *Interfacial Phenomena in Metals and Alloys*. (Addison-Wesley Publishing Co., 1975).

16 deBoer, F. R., Boom, B., Mattens, W. C. M., Miedema, A. R. & Niessen, A. K. *Cohesion in Metals: Transition Metal Alloys*. (Elsevier Science Publishers, 1989).

17 Franke, P. & Neuschutz, D. *Thermodynamic Properties of Inorganic Materials compiled by SGTE*. Vol. Volume 19; Subvolume B; Binary Systems; Phase Diagrams, Phase Transition Data, Integral and Partial Quantities of Alloys (ed W. Martienssen) (Springer-Verlag, Berlin, Germany, 2002).

18 Hultgren, R., Orr, R. L., Anderson, P. D. & Kelley, K. K. *Selected Values of Thermodynamic Properties of Metals and Alloys*. (John Wiley & Sons, Inc., 1963).

19 Kubaschewski, O., Alcock, C. B. & Spencer, P. J. *Materials Thermochemistry, 6th Edition*. (Pergamon Press, Oxford, UK, 1993).

[20] Pauling, L. *The nature of the chemical bond*. Third edn, (Cornell University Press, 1960).

[21] Lad, K. N. & Pratap, A. Phonon dispersion in amorphous Zr–Ni alloys. *Physica B* **334**, 135-146 (2003).

[22] Guerdane, M. & Teichler, H. Structure of the amorphous, massive-metallic-glass forming $Ni_{25}Zr_{60}Al_{15}$ alloy from molecular dynamics simulations. *Phys. Rev. B* **65**, 014203 (2001).

[23] Gu, X. J., Poon, S. J., Shiflet, G. J. & Widom, M. Ductility improvement of amorphous steels: Roles of shear modulus and electronic structure. *Acta mater.* **56**, 88-94 (2008).

[24] Gu, X. J., Poon, S. J., Shiflet, G. J. & Widom, M. Mechanical properties, glass transition temperature, and bond enthalpy trends of high metalloid Fe-based bulk metallic glasses. *Appl. Phys. Lett.* **92**, 161910 (2008).

[25] Hirth, J. P. & Lothe, J. *Theory of Dislocations*. 2nd edn, (Krieger Publishing Co., 1992).

[26] Yeh, J.-W. Recent progress in high entropy alloys. *Ann. Chim. Sci. Mat.* **31**, 633-648 (2006).

[27] Inoue, A. Stabilization of metallic supercooled liquid and bulk amorphous alloys. *Acta mater.* **48**, 279-306 (2000).

[28] Wang, W. H., Dong, C. & Shek, C. H. Bulk metallic glasses. *Mat. Sci. Eng.* **R44**, 45-89 (2004).

[29] Angell, C. A. Formation of glasses from liquids and biopolymers. *Science* **267**, 1924-1935 (1995).

[30] Ashcroft, N. W. & Mermin, N. D. *Solid State Physics*. 396 (Brooks Cole, 1976).

[31] Friedel, J. The distribution of electrons round impurities in monovalent metals. *Phil. mag.* **43**, 153-189 (1952).

[32] Okamoto, H., Subramanian, P. R. & Kacprzak, L. *Binary Alloy Phase Diagrams*. 2nd edn, (ed T.B. Massalski) (ASM, International, 1990).

[33] Villars, P. & Calvert, L. D. *Pearson's Handbook of Crystallographic Data for Intermetallic Phases*. (ASM, International, 1991).

[34] Daams, J. L. C., P.Villars & Vucht, J. H. N. v. *Atlas of Crystal Structure Types for Intermetallic Phases*. (ASM, International, 1991).

[35] Lee, B.-J., Shim, J.-H. & Baskes, M. I. Semiempirical atomic potentials for the fcc metals Cu, Ag, Au, Ni, Pd, Pt, Al, and Pb based on first and second nearest-neighbor modified embedded atom method. *Phys. Rev. B* **68**, 144112 (2003).

[36] Miedema, A. R. The formation enthalpy of monovacancies in metals and intermetallic compounds. *Z. Metallkde.* **70**, 345-353 (1979).

[37] Triftshauser, W. & McGervey, J. D. Monovacancy formation energy in copper, silver, and gold by positron annihilation. *Appl. Phys.* **6**, 177-180 (1975).

[38] Wolff, J., Franz, M., Kluin, J.-E. & Schmid, D. Vacancy formation in nickel and α-nickel-carbon alloy. *Acta mater.* **45**, 4759-4764 (1997).

[39] Hu, R. & Nash, P. Review: Experimental enthalpies of formation of compounds in Al-Ni-X systems. *J. Mater. Sci.* **41**, 631-641 (2006).

[40] Miracle, D. B., Louzguine-Luzgin, D., Louzguina-Luzgina, L. & Inoue, A. An assessment of binary metallic glasses: Correlations between structure, glass forming ability and stability. *International Materials Review* (Accepted for publication).

Supplementary Information accompanies the paper on **www.nature.com/nature**.

Acknowledgements We thank P. Harrowell, R. Busch, M. Widom, D. Nicholson and C. Woodward for helpful comments. This work was supported by a grant from the Air Force Office of Scientific Research (M. Berman, Program Manager).

Author Contributions D.M. conceived and conducted the work and wrote the paper. G.W. performed analysis and wrote the section regarding inter-relation between bond enthalpies, bond fractions and topology, and edited the manuscript. J.D. and A.D. collected and analysed the thermodynamic data and edited the manuscript.

Author Information Reprints and permissions information is available at npg.nature.com/reprintsandpermissions. The authors declare no competing financial interests. Correspondence and requests for materials should be addressed to D.M. (daniel.miracle@wpafb.af.mil).

Table 1 Elemental condensed bond enthalpies, ε_{AA}

Element	Atomic Number	ε_{AA} (eV)	Element	Atomic Number	ε_{AA}· (eV)	Element	Atomic Number	ε_{AA}· (eV)
H	1	-2.26±0.00001	As	33	-1.05±0.045	Tb	65	-0.671±0.004
Li	3	-0.236±0.002	Se	34	-1.57±0.028	Dy	66	-0.502±0.004
Be	4	-0.560±0.009	Br	35	-1.16±0.001	Ho	67	-0.519±0.004
B	5	-1.80±0.016	Rb	37	-0.120±0.001	Er	68	-0.547±0.004
C	6	-4.95±0.003	Sr	38	-0.283±0.003	Tm	69	-0.401±0.004
N	7	-4.90±0.004	Y	39	-0.734±0.004	Yb	70	-0.269±0.004
O	8	-2.58±0.001	Zr	40	-1.05±0.015	Lu	71	-0.739±0.004
F	9	-0.823±0.003	Nb	41	-1.09±0.012	Hf	72	-1.07±0.011
Na	11	-0.159±0.001	Mo	42	-0.976±0.006	Ta	73	-1.16±0.004
Mg	12	-0.254±0.001	Tc	43	-1.17±0.023	W	74	-1.26±0.009
Al	13	-0.572±0.007	Ru	44	-1.12±0.011	Re	75	-1.34±0.011
Si	14	-2.33±0.042	Rh	45	-0.960±0.007	Os	76	-1.36±0.011
P	15	-2.19±0.007	Pd	46	-0.651±0.004	Ir	77	-1.16±0.007
S	16	-2.87±0.002	Ag	47	-0.492±0.001	Pt	78	-0.977±0.002
Cl	17	-1.26±0.0001	Cd	48	-0.193±0.003	Au	79	-0.636±0.004
K	19	-0.132±0.001	In	49	-0.420±0.007	Hg	80	-0.106±0.0001
Ca	20	-0.307±0.001	Sn	50	-0.624±0.003	Tl	81	-0.315±0.001
Sc	21	-0.653±0.013	Sb	51	-0.914±0.009	Pb	82	-0.337±0.001
Ti	22	-0.817±0.005	Te	52	-1.36±0.015	Bi	83	-0.483±0.005
V	23	-0.763±0.012	I	53	-1.11±0.004	Po	84	-0.491±0.010
Cr	24	-0.589±0.006	Cs	55	-0.113±0.002	Ra	88	-0.235±0.005
Mn	25	-0.448±0.007	Ba	56	-0.265±0.007	Ac	89	-0.701±0.014
Fe	26	-0.615±0.002	La	57	-0.745±0.004	Th	90	-1.04±0.010
Co	27	-0.737±0.015	Ce	58	-0.726±0.004	Pa	91	-0.834±0.017
Ni	28	-0.743±0.015	Pr	59	-0.617±0.004	U	92	-0.921±0.014
Cu	29	-0.583±0.002	Nd	60	-0.565±0.004	Np	93	-0.642±0.013
Zn	30	-0.225±0.001	Sm	62	-0.357±0.004	Pu	94	-0.511±0.010
Ga	31	-0.805±0.006	Eu	63	-0.263±0.003			
Ge	32	-1.93±0.016	Gd	64	-0.687±0.004			

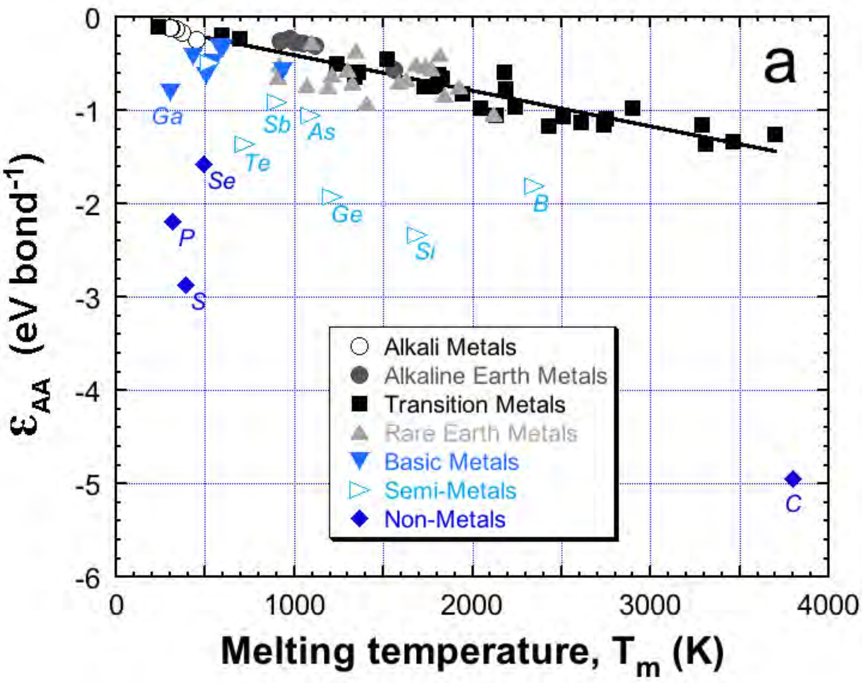

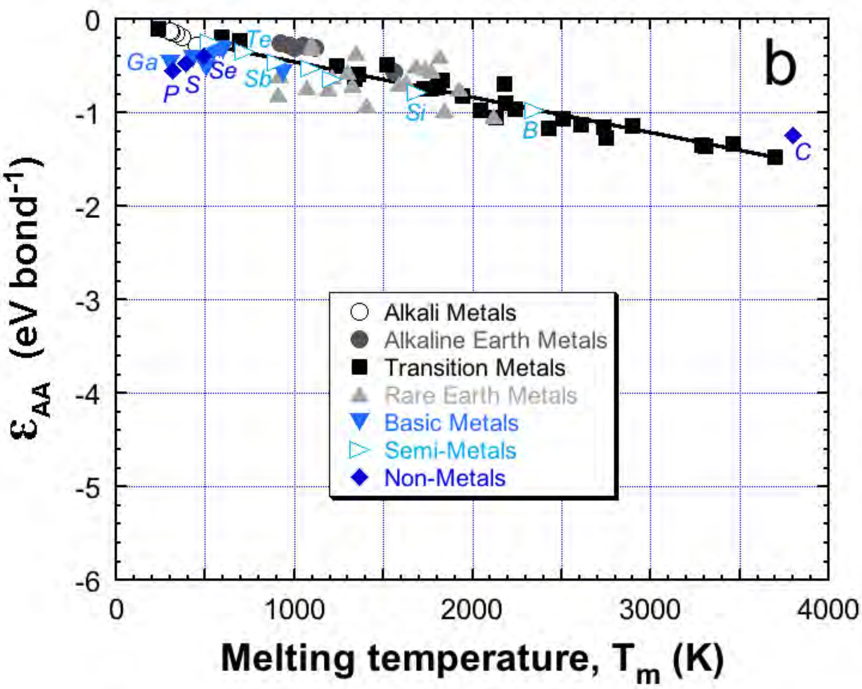

Figure 1 | Elemental condensed bond enthalpies vs melting temperature, T_m. *a* Condensed bond enthalpies calculated using coordination numbers of the equilibrium structures. *b* Condensed bond enthalpies calculated using a space-filling coordination number of 12 for all elements.

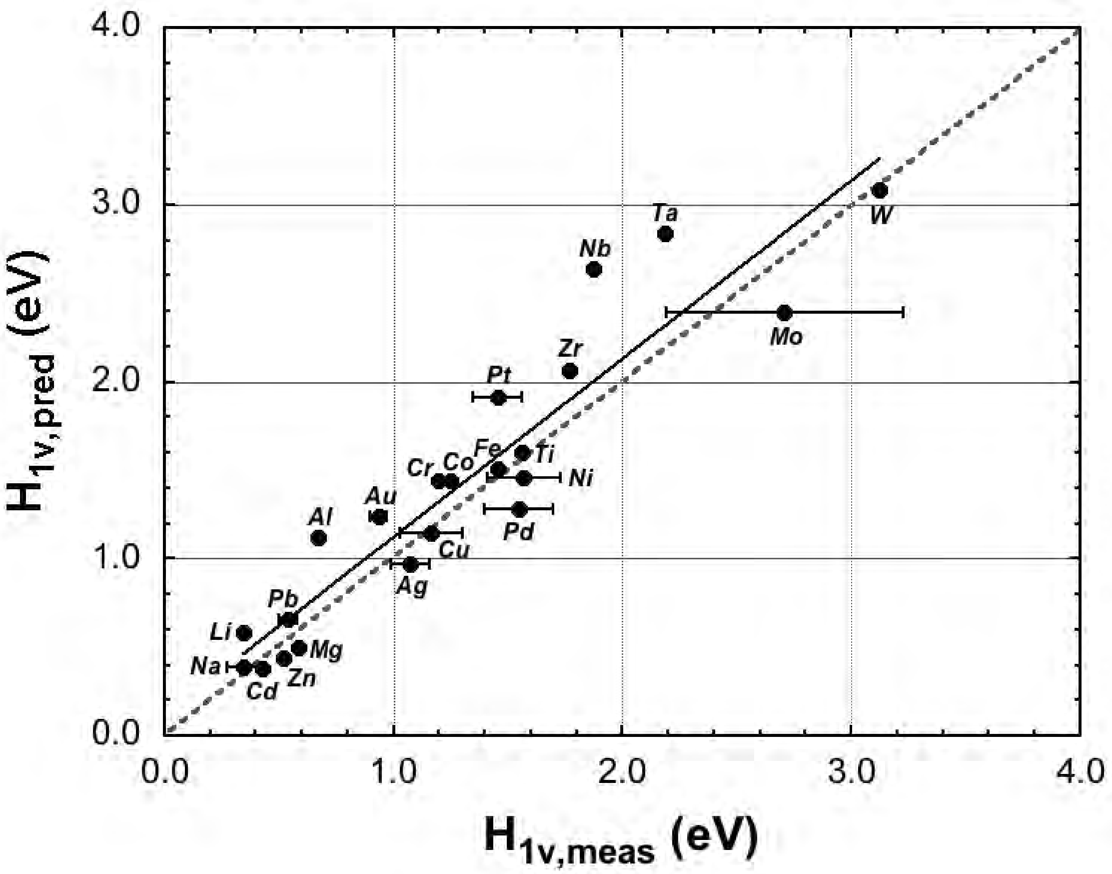

Figure 2 | Measured and predicted monovacancy formation energies in metallic elements. The solid line is a least-squares fit and the dotted line represents perfect agreement. The error bars give the reported range in experimental values for the elements indicated. Bond enthalpy estimates exceed measured values by about 0.1 eV, within typical experimental error. Experimental data are from [35,36,37,38].

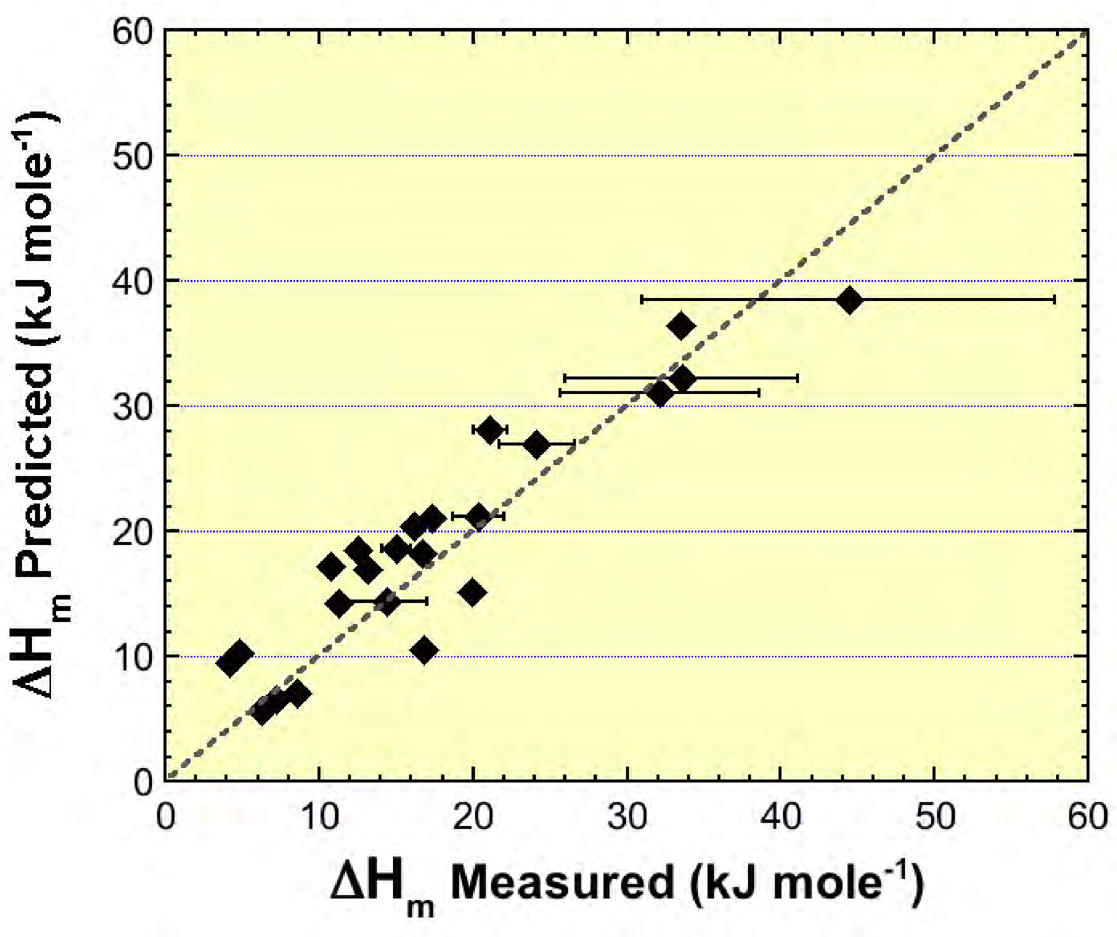

Figure 3 | Measured and predicted enthalpies of fusion for metallic elements. The dotted line represents perfect agreement. Error bars show ranges in experimental values, taken from [4,5].

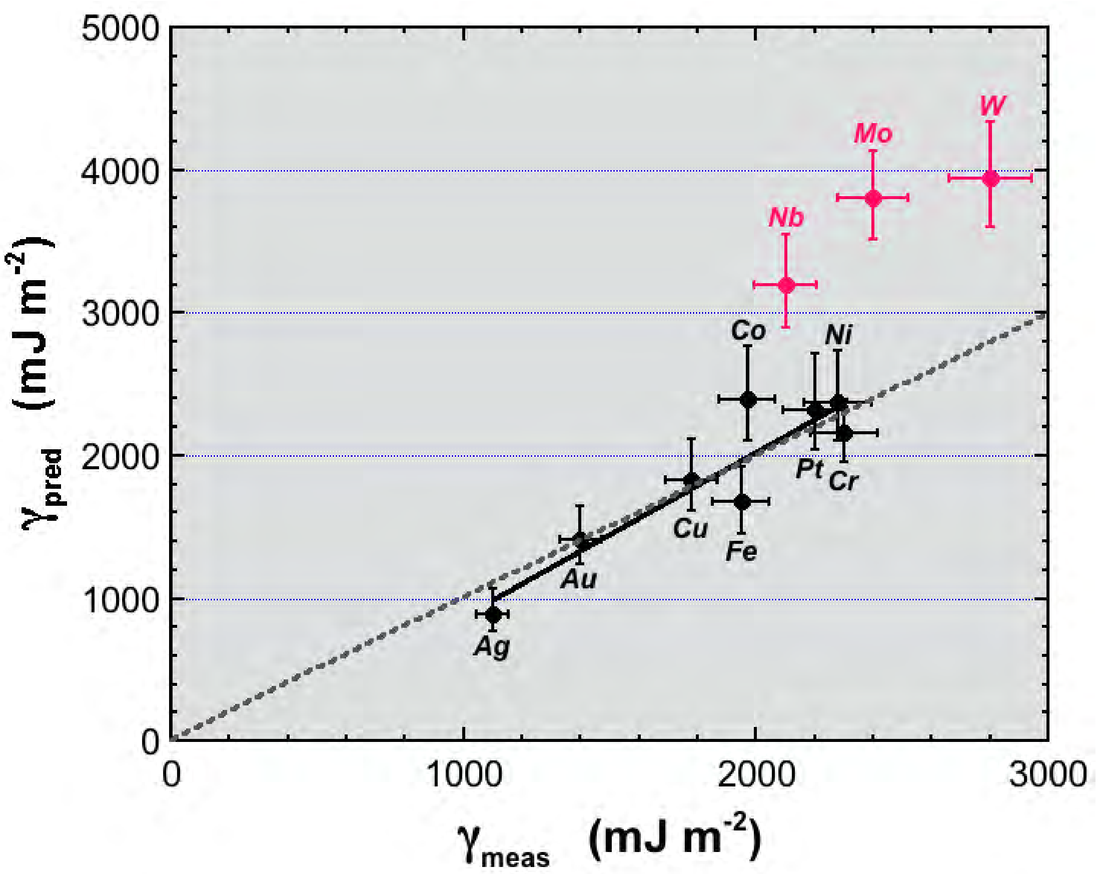

Figure 4 | Comparison of measured and predicted solid surface energies, γ. Error bars for predicted data give the range in values predicted for the different crystallographic planes. A modest error of ±5% is assumed for measured values. The solid line is a linear regression for elements where measurements are made at ≤ 1723 K, and the dotted line represents perfect agreement. Measurements for Nb, Mo and W are made at much higher temperatures, where impurity adsorption may alter surface energies. Experimental data are taken from [15].

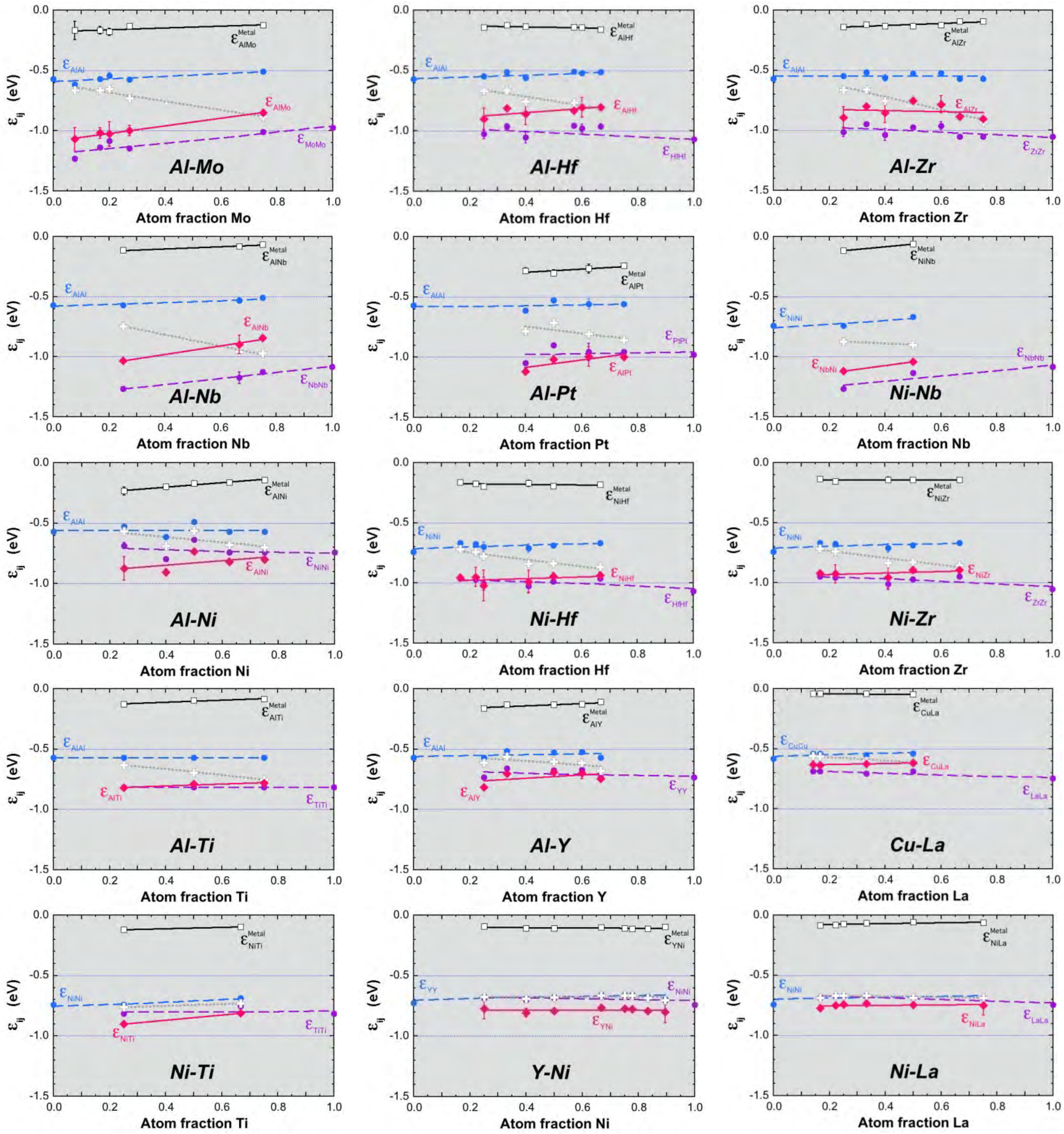

Figure 5 | For each binary system are plotted: ε_{AA} for element A (at atom fraction B = 0) and in the binary compounds; ε_{BB} for element B (at atom fraction B = 1) and in the binary compounds; and ε_{AB} relative to both the gas and 'elemental' standard states. The compositionally-weighted averages of $\varepsilon_{AA}^{A_xB_y}$ and $\varepsilon_{BB}^{A_xB_y}$ are shown by open crosses. The more negative ε_{ii} of the two elements is B in all plots.

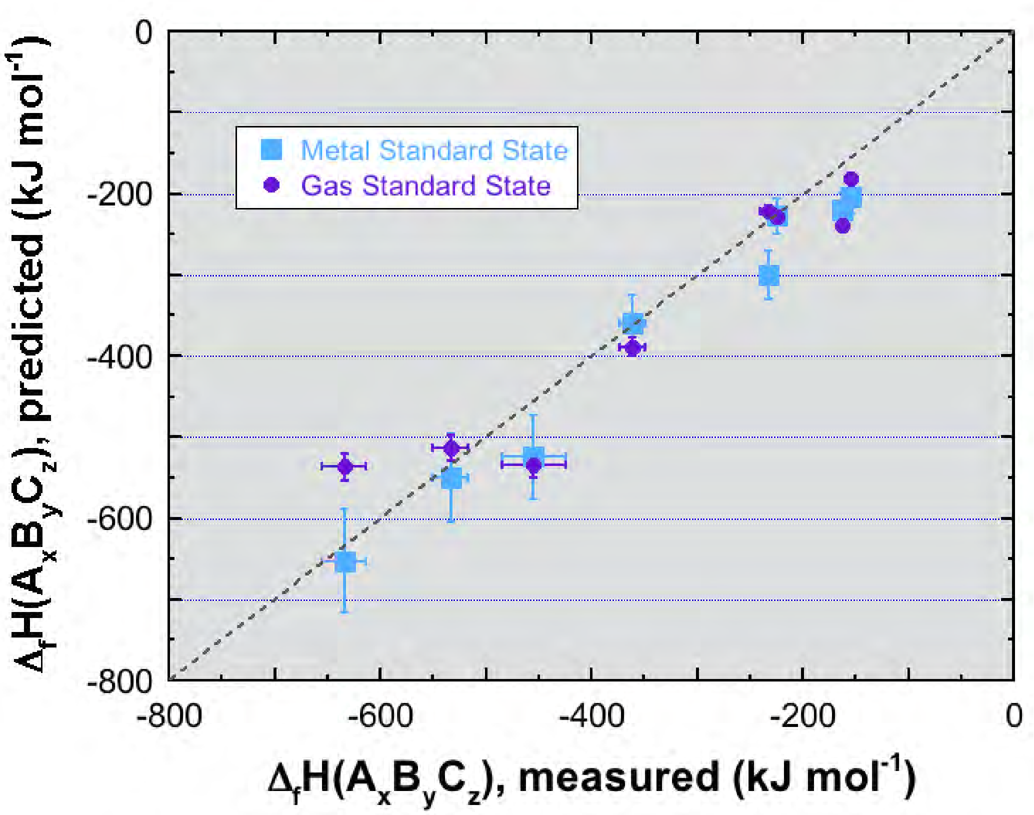

Figure 6 | Comparison of measured and predicted enthalpies of formation for ternary compounds, $\Delta_f H(A_xB_yC_z)$. Predictions are made using $\varepsilon_{ii}^{A_xB_y}$ and with ε_{ij} values relative to both the gas and metal standard states. The dotted line represents perfect agreement. Experimental data are taken from [39].

SUPPLEMENTARY INFORMATION

Table S1 Elemental bond enthalpies, ε_{AA}

Element	$\Delta_f H$(gas) (kJ mol^{-1}) *	P_{AA}	ε_{AA} (eV)	Element	$\Delta_f H$(gas) (kJ mol^{-1}) *	P_{AA}	ε_{AA} (eV)
H	217.998±0.0006	1	-2.26±0.00001	Cd	111.8±0.2	6	-0.193±0.003
Li	159.3±1.0	7	-0.236±0.002	In	243±4	6	-0.420±0.007
Be	324±5	6	-0.560±0.009	Sn	301.2±1.5	5	-0.624±0.003
B	565±5	3.25	-1.80±0.016	Sb	264.4±2.5	3	-0.914±0.009
C	716.68±0.45	1.5	-4.95±0.003	Te	196.6±2.1	1.5	-1.36±0.015
N	472.68±0.4	1	-4.90±0.004	I	106.76±0.04	1	-1.11±0.004
O	249.229±0.0002	1	-2.58±0.001	Cs	76.5±1.0	7	-0.113±0.002
F	79.38±0.3	1	-0.823±0.003	Ba	179.1±5.0	7	-0.265±0.007
Na	107.5±0.7	7	-0.159±0.001	La	431±2.1	6	-0.745±0.004
Mg	147.1±0.8	6	-0.254±0.001	Ce	420.1±2.1	6	-0.726±0.004
Al	330.9±4	6	-0.572±0.007	Pr	356.9±2.1	6	-0.617±0.004
Si	450±8	2	-2.33±0.042	Nd	326.9±2.1	6	-0.565±0.004
P	316.5±1.0	1.50	-2.19±0.007	Sm	206.7±2.1	6	-0.357±0.004
S	277.17±0.15	1	-2.87±0.002	Eu	177.4±2.1	7	-0.263±0.003
Cl	121.301±0.008	1	-1.26±0.0001	Gd	397.5±2.1	6	-0.687±0.004
K	89±0.8	7	-0.132±0.001	Tb	388.7±2.1	6	-0.671±0.004
Ca	177.8±0.8	6	-0.307±0.001	Dy	290.4±2.1	6	-0.502±0.004
Sc	377.8±4	6	-0.653±0.013	Ho	300.6±2.1	6	-0.519±0.004
Ti	473±3	6	-0.817±0.005	Er	316.4±2.1	6	-0.547±0.004
V	515.5±8	7	-0.763±0.012	Tm	232.2±2.1	6	-0.401±0.004
Cr	397.48±4.2	7	-0.589±0.006	Yb	155.6±2.1	6	-0.269±0.004
Mn	283.3±4.2	6.55	-0.448±0.007	Lu	427.6±2.1	6	-0.739±0.004
Fe	415.5±1.3	7	-0.615±0.002	Hf	618.4±6.3	6	-1.07±0.011
Co	426.7±8.5	6	-0.737±0.015	Ta	782±2.5	7	-1.16±0.004
Ni	430.1±8.4	6	-0.743±0.015	W	851±6.3	7	-1.26±0.009
Cu	337.4±1.2	6	-0.583±0.002	Re	774±6.3	6	-1.34±0.011
Zn	130.4±0.4	6	-0.225±0.001	Os	787±6.3	6	-1.36±0.011
Ga	271.96±2.1	3.5	-0.805±0.006	Ir	669±4	6	-1.16±0.007
Ge	372±3	2	-1.93±0.016	Pt	565.7±1.3	6	-0.977±0.002
As	302.5±13	3	-1.05±0.045	Au	368.2±2.1	6	-0.636±0.004
Se	227.2±4	1.5	-1.57±0.028	Hg	61.38±0.04	6	-0.106±0.0001
Br	111.87±0.1	1	-1.16±0.001	Tl	182.2±0.4	6	-0.315±0.001
Rb	80.9±0.8	7	-0.120±0.001	Pb	195.2±0.8	6	-0.337±0.001
Sr	164±1.7	6	-0.283±0.003	Bi	209.6±2.1	4.5	-0.483±0.005
Y	427.4±2.1	6	-0.734±0.004	Po	142±2.8	3	-0.491±0.010
Zr	610±8.4	6	-1.05±0.015	Ra	159±3.2	7	-0.235±0.005
Nb	733±8	7	-1.09±0.012	Ac	406±8.1	6	-0.701±0.014
Mo	658.98±3.8	7	-0.976±0.006	Th	602±6	6	-1.04±0.010
Tc	678±13.6	6	-1.17±0.023	Pa	563±11.3	7	-0.834±0.017
Ru	650.6±6.3	6	-1.12±0.011	U	533±8	6	-0.921±0.014
Rh	556±4	6	-0.960±0.007	Np	464.8±9.3	7.5	-0.642±0.013
Pd	376.6±2.1	6	-0.651±0.004	Pu	345±6.9	7	-0.511±0.010
Ag	284.9±0.8	6	-0.492±0.001				

* Assessed from values reported in [4,5,11,12].

Table S2 Bonds broken per unit area, Б

Plane and structure	Б
$(100)_{fcc}$	$\frac{1}{2r^2}$
$(110)_{fcc}$	$\frac{3}{4\sqrt{2}r^2}$
$(111)_{fcc}$	$\frac{3}{4\sqrt{3}r^2}$
$(100)_{bcc}$	$\frac{9}{16r^2}$
$(110)_{bcc}$	$\frac{3}{4\sqrt{2}r^2}$
$(112)_{bcc}$	$\frac{\sqrt{3}}{2\sqrt{2}r^2}$

Table S3 Measured and calculated surface energies

Element	γ_{meas} [a] ($mJ m^{-2}$)	dF_S / dT ($mJ\ m^{-2}\ K^{-1}$)	T_{meas} (K)	H_T-H_{298} ($J\ mol^{-1}$)	$\Delta(H_T - H_{298}) / \Delta T$ ($J\ mol^{-1} K^{-1}$)	γ_{100} ($mJ m^{-2}$)	γ_{110} ($mJ m^{-2}$)	γ_{111} ($mJ m^{-2}$)	γ_{112} ($mJ m^{-2}$)
Ag	1100	-0.47	1223	26077	31.38	833	1071	769	
Au	1400	-0.43	1273	27041	30.54	1339	1645	1243	
Cu	1780	-0.50	1198	24606	29.50	1759	2117	1618	
Fe	1950	-0.90	1723	55094	41.42	1641	1458		1924
Co	1970	-0.52 [b]	1627	49064	39.75	2329	2764	2101	
Nb	2100	-0.52 [b]	2523	65380	33.89	3150	2894		3546
Pt	2200	-0.60	1573	37319	32.64	2219	2711	2040	
Ni	2280	-0.55	1333	33195	35.35	2286	2739	2102	
Cr	2300	-0.52 [b]	1673	44590	42.26	2128	1956		2394
Mo	2400	-0.20	2623	73976	40.17	3759	3514		4139
W	2800	-0.52 [b]	2273	55679	31.38	3888	3598		4337

[a] From [15]).

[b] Estimated as the average of the measured values.

Table S4 Calculated values of ε_{AB}

Compound A_xB_y	Pearson Symbol (Prototype)	A–A bonds per unit cell [a]	A–B bonds per unit cell [a]	B–B bonds per unit cell [a]	Δ_fH (A_xB_y) [b] (kJ mole^{-1})	$\varepsilon_{AA}^{A_xB_y}$ (eV bond^{-1})	$\varepsilon_{BB}^{A_xB_y}$ (eV bond^{-1})	ε_{AB} (eV bond^{-1})
Al_3Hf	tI16 (Al_3Zr)	48	48	4	-168±14	-0.549±0.021	-1.03±0.039	-0.902±0.090
Al_2Hf	hP12 ($MgZn_2$)	24	48	8	-144±12	-0.514±0.007	-0.961±0.011	-0.813±0.018
Al_3Hf_2	oF40 (Al_3Zr_2)	48	148	48	-240±20	-0.562±0.026	-1.05±0.049	-0.860±0.081
Al_3Hf_4	hP7 (Al_3Zr_4)	6	24	17	-322±27	-0.511±0.007	-0.955±0.011	-0.832±0.019
Al_2Hf_3	tP20 (Al_2Zr_3)	8	64	59	-220±18	-0.524±0.019	-0.979±0.036	-0.805±0.070
$AlHf_2$	tI12 (Al_2Cu)	4	32	44	-123±10	-0.514±0.007	-0.961±0.011	-0.804±0.019
$Al_{12}Mo$	cI26 ($Al_{12}W$)	12	1	13	-195±87	-0.619±0.007	-1.23±0.006	-1.07±0.085
Al_5Mo	hP12 (Al_5W)	5	1	6	-192±35	-0.572±0.007	-1.14±0.006	-1.02±0.037
Al_4Mo	mC30 (Al_4W)	4	1	5	-185±29	-0.544±0.025	-1.08±0.049	-1.03±0.092
Al_8Mo_3	mC22 (Al_8Mo_3)	8	3	11	-484±41	-0.576±0.007	-1.15±0.009	-1.02±0.036
$AlMo_3$	cP8 (Cr_3Si)	1	3	4	-142±15	-0.508±0.007	-1.01±0.006	-0.851±0.019
Al_3Nb	tI8 (Al_3Ti)	24	24	0	-132±11	-0.572±0.007	-1.27±0.012	-1.03±0.020
$AlNb_2$	tP30 (CrFe)	12	94	88	-75±6	-0.530±0.021	-1.18±0.047	-0.896±0.077
$AlNb_3$	cP8 (Cr_3Si)	0	24	30	-76±6	-0.508±0.007	-1.13±0.012	-0.844±0.015
Al_3Ni	oP16 (CFe_3)	68	34	2	-192±16	-0.573±0.020	-0.686±0.025	-0.874±0.096
Al_3Ni_2	hP5 (Al_3Ni_2)	9	16	3	-306±26	-0.612±0.007	-0.796±0.015	-0.905±0.029
AlNi	cP2 (CsCl)	3	8	3	-132±11	-0.490±0.007	-0.637±0.015	-0.734±0.022
Al_3Ni_5	oC16 (Ga_3Pt_5)	8	56	32	-435±37	-0.572±0.007	-0.743±0.015	-0.818±0.024
$AlNi_3$	cP4 ($AuCu_3$)	0	12	12	-164±14	-0.572±0.007	-0.743±0.015	-0.799±0.023
Al_3Pt_2	hP5 (Al_3Ni_2)	9	16	3	-435±37	-0.612±0.007	-1.05±0.022	-1.12±0.029
AlPt	cP8 (FeSi)	12	28	12	-204±17	-0.528±0.007	-0.902±0.022	-1.02±0.029
Al_3Pt_5	oP16 (Ge_3Rh_5)	5	55	38	-704±59	-0.560±0.042	-0.957±0.072	-0.993±0.081
$AlPt_3$	tP16 ($GaPt_3$)	0	48	50	-280±24	-0.560±0.007	-0.957±0.022	-0.996±0.025
Al_3Ti	tI8 (Al_3Ti)	24	24	0	-147±3	-0.572±0.007	-0.817±0.005	-0.821±0.008
AlTi	tP4 (AuCu)	4	16	4	-74±2	-0.572±0.007	-0.817±0.005	-0.790±0.009
$AlTi_3$	hP8 (Ni_3Sn)	0	24	24	-100±8	-0.572±0.007	-0.817±0.005	-0.781±0.013
Al_3Y	hP8 (Ni_3Sn)	24	24	0	-190±16	-0.572±0.007	-0.734±0.004	-0.817±0.019
Al_2Y	cF24 (Cu_2Mg)	48	96	16	-151±13	-0.514±0.007	-0.660±0.004	-0.702±0.016
AlY	oC8 (BCr)	4	28	20	-90±8	-0.528±0.007	-0.677±0.004	-0.693±0.017
Al_2Y_3	tP20 (Al_2Zr_3)	8	64	59	-200±17	-0.524±0.019	-0.672±0.025	-0.699±0.048
AlY_2	oP12 (Co_2Si)	0	40	32	-105±9	-0.572±0.007	-0.734±0.004	-0.745±0.015
Al_3Zr	tI16 (Al_3Zr)	48	48	4	-163±14	-0.549±0.021	-1.01±0.039	-0.892±0.089
Al_2Zr	hP12 ($MgZn_2$)	24	48	8	-137±12	-0.514±0.007	-0.948±0.015	-0.802±0.018
Al_3Zr_2	oF40 (Al_3Zr_2)	48	148	48	-235±20	-0.562±0.026	-1.04±0.049	-0.853±0.082
AlZr	oC8 (BCr)	4	28	20	-89±7	-0.528±0.007	-0.973±0.015	-0.755±0.018
Al_2Zr_3	tP20 (Al_2Zr_3)	8	64	59	-192±16	-0.524±0.019	-0.965±0.036	-0.783±0.072
$AlZr_2$	hP6 ($InNi_2$)	0	22	14	-100±8	-0.572±0.007	-1.05±0.015	-0.885±0.018

$AlZr_3$	cP4 ($AuCu_3$)	0	12	12	-108±9	-0.572±0.007	-1.05±0.015	-0.906±0.019
Cu_6La	oP28 ($CeCu_6$)	106	76	0	-79±11	-0.538±0.017	-0.687±0.022	-0.632±0.030
Cu_5La	hP6 ($CaCu_5$)	21	18	0	-75±3	-0.538±0.021	-0.687±0.036	-0.635±0.004
Cu_2La	hP3 (AlB_2)	3	12	4	-51±3	-0.552±0.021	-0.705±0.036	-0.626±0.005
CuLa	oP8 (BFe)	4	28	20	-32±3	-0.538±0.021	-0.687±0.036	-0.617±0.006
$HfNi_5$	cF24 ($AuBe_5$)	96	64	0	-252±21	-0.669±0.015	-0.961±0.011	-0.954±0.023
Hf_2Ni_7	mC36 (Ni_7Zr_2)	112	112	14	-468±39	-0.674±0.017	-0.970±0.024	-0.950±0.073
α-$HfNi_3$	hR12 ($BaPb_3$)	36	36	4.5	-228±19	-0.699±0.039	-1.01±0.056	-1.02±0.124
Hf_7Ni_{10}	oC68 ($Ni_{10}Zr_7$)	80	258	88	-1071±90	-0.712±0.035	-1.02±0.050	-0.989±0.088
HfNi	oC8 (BCr)	4	28	20	-130±11	-0.686±0.015	-0.986±0.011	-0.943±0.028
Hf_2Ni	tI12 (Al_2Cu)	4	32	44	-141±12	-0.669±0.015	-0.961±0.011	-0.937±0.026
$LaNi_5$	hP6 ($CaCu_5$)	21	18	0	-148±21	-0.686±0.015	-0.687±0.004	-0.772±0.021
La_2Ni_7	hP36 (Ce_2Ni_7)	108	120	12	-234±20	-0.669±0.015	-0.670±0.004	-0.750±0.015
$LaNi_3$	hR12 (Be_3Nb)	33	42	5	-98±14	-0.669±0.015	-0.670±0.04	-0.742±0.019
$LaNi_2$	cF24 (Cu_2Mg)	48	96	16	-75±15	-0.669±0.015	-0.670±0.004	-0.734±0.021
LaNi	oC8 (BCr)	4	28	20	-40±3	-0.686±0.015	-0.687±0.004	-0.745±0.016
La_3Ni	oP16 (CFe_3)	2	34	68	-52±4	-0.686±0.025	-0.687±0.026	-0.750±0.056
$NbNi_3$	oP8 (Cu_3Ti)	24	24	0	-133±11	-0.743±0.015	-1.27±0.012	-1.12±0.024
Nb_7Ni_6	hR13 (Fe_7W_6)	18	48	21	-281±24	-0.666±0.015	-1.14±0.012	-0.979±0.017
Ni_3Ti	hP16 (Ni_3Ti)	48	48	0	-140±12	-0.743±0.015	-0.817±0.005	-0.901±0.020
$NiTi_2$	cF96 ($NiTi_2$)	48	288	288	-83±2	-0.686±0.015	-0.754±0.005	-0.811±0.011
NiY_3	oP16 (CFe_3)	68	34	2	-76±6	-0.677±0.025	-0.686±0.025	-0.776±0.060
Ni_2Y_3	tP80 (Ni_2Y_3)	256	228	24	-150±13	-0.693±0.005	-0.702±0.015	-0.809±0.033
NiY	oP8 (BFe)	20	28	4	-74±6	-0.677±0.004	-0.686±0.015	-0.794±0.020
Ni_2Y	cF24 (Cu_2Mg)	16	96	48	-117±10	-0.660±0.004	-0.669±0.015	-0.767±0.017
Ni_3Y	hR12 (Be_3Nb)	5	42	33	-148±12	-0.660±0.004	-0.669±0.015	-0.775±0.018
Ni_7Y_2	hR18 (Co_7Er_2)	6	60	54	-315±26	-0.660±0.004	-0.669±0.015	-0.775±0.017
Ni_5Y	hP6 ($CaCu_5$)	0	18	21	-195±9	-0.677±0.004	-0.686±0.015	-0.795±0.014
$Ni_{17}Y_2$	hP38 ($Ni_{17}Th_2$)	0	76	164	-361±30	-0.697±0.033	-0.706±0.034	-0.801±0.087
Ni_5Zr	cF24 ($AuBe_5$)	96	64	0	-210±18	-0.669±0.015	-0.948±0.015	-0.921±0.022
Ni_7Zr_2	mC36 (Ni_7Zr_2)	112	112	14	-414±35	-0.674±0.017	-0.956±0.024	-0.926±0.073
$Ni_{10}Zr_7$	oC68 ($Ni_{10}Zr_7$)	80	258	88	-884±74	-0.712±0.035	-1.01±0.050	-0.955±0.085
NiZr	oC8 (BCr)	4	28	20	-98±8	-0.686±0.015	-0.973±0.015	-0.892±0.025
$NiZr_2$	tI12 (Al_2Cu)	4	32	44	-111±9	-0.669±0.015	-0.948±0.015	-0.894±0.023

[a] From [34].

[b] Assessed from values reported in [16,17,18,19].

Table S5 Measured and calculated ternary compound heats of formation

Compound $A_xB_yC_z$	Pearson Symbol (Prototype)	A–A bonds per unit cell	A–B bonds per unit cell	A–C bonds per unit cell	B–B bonds per unit cell	B–C bonds per unit cell	C–C bonds per unit cell	Δ_fH ($A_xB_yC_z$), measured [a] (kJ mole^{-1})	Δ_fH ($A_xB_yC_z$), predicted [b] (kJ mole^{-1})	Δ_fH ($A_xB_yC_z$), predicted [c] (kJ mole^{-1})
$AlNi_2Hf$	cF16 (BiF_3)	0	32	24	24	32	0	-233±7	-221±7	-301±30
$Al_3Ni_{12}Hf$	cP4 ($AuCu_3$)	0	9	0	12	3	0	-634±21	-537±16	-652±64
$AlNi_2Nb$	cF16 (BiF_3)	0	32	24	24	32	0	-154±4	-181±5	-204±20
$AlNi_2Ti$	cF16 (BiF_3)	0	32	24	24	32	0	-224	-228±7	-228±22
AlNiY	hP9 (Fe_2P)	3	12	18	0	15	6	-162±3	-239±7	-220±22
Al_4NiY	oC24 (Al_4NiY)	52	28	48	0	12	4	-362±12	-389±12	-360±35
$AlNi_8Y_3$	hP24 ($CeNi_3$)	0	18	6	48	78	10	-455±30	-535±16	-524±51
$Al_2Ni_6Y_3$	cI44 (Ag_8Ca_3)	0	48	48	72	96	24	-534±17	-513±15	-550±54

[a] From [39].

[b] Gas standard state.

[c] Metal standard state.

Table S6 Second-neighbour contribution to ε_{ii}

Element	Stacking Fault Energy (mJ m^{-2}) [a]	ε_{ii}^{SFE} (eV bond^{-1})	$\varepsilon_{ii}^{SFE}/\varepsilon_{ii}$
Ag	16	0.0024	0.0049
Al	166	0.0238	0.0416
Au	32	0.0047	0.0074
Cd	175	0.0311	0.1610
Cu	45	0.0051	0.0088
Ir	300	0.0400	0.0346
Mg	125	0.0231	0.0908
Ni	125	0.0143	0.0193
Pd	180	0.0262	0.0402
Pt	322	0.0448	0.0459
Rh	750	0.0942	0.0981
	115	0.0263	0.0253
Zn	140	0.0198	0.0878

[a] From [25].

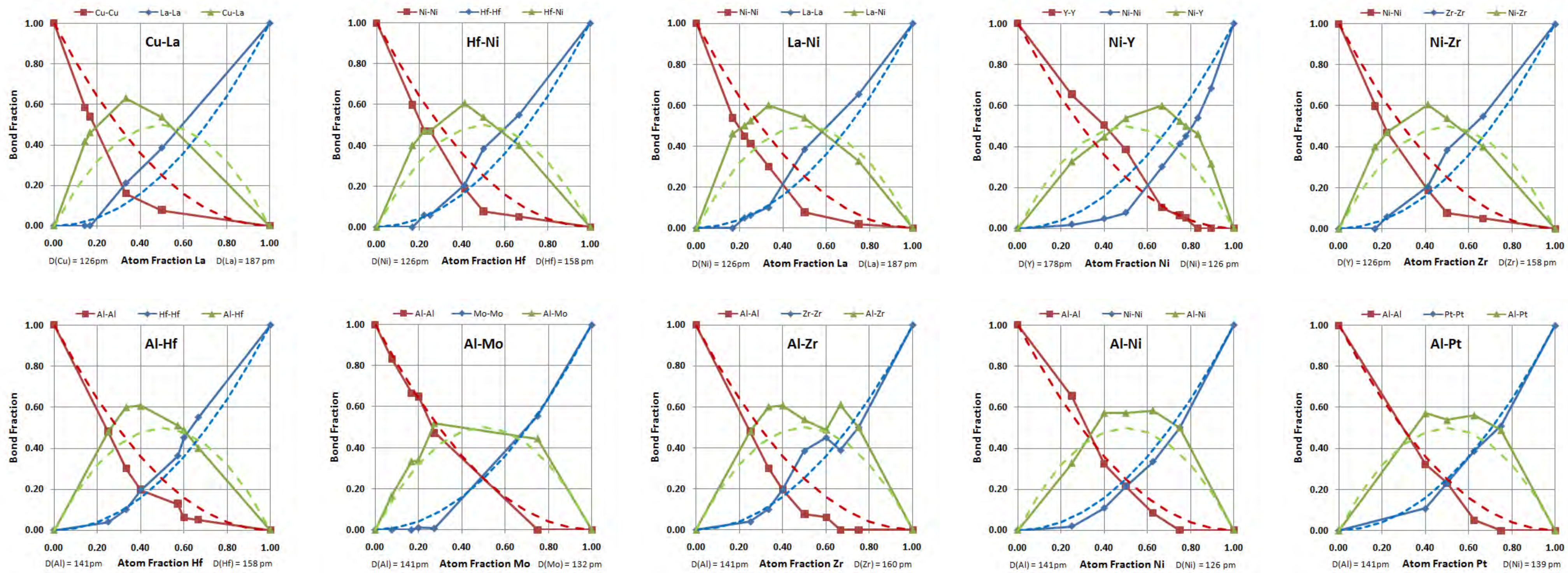

Figure S1 | Fractions of A–A, A–B, and B–B bonds for selected binary systems as a function of atom fraction of element B (f_B). Element B, where $\varepsilon_{BB} < \varepsilon_{AA}$, is on the right hand side of each binary system. Dashed lines indicate the bond concentrations expected for an ideal solution of equal-sized atoms. Constituent atom sizes [40] are included in each figure—note the universal skewing of A–B bonds towards the smaller constituent.